ART & TECHNOLOGY PUBLISHING PTE. LTD.

Materials Science Advanced Composite Materials

2023 Volume 1, Issue 1

ISSN: 2529-7783

Characteristics of Spark Plasma Sintered Nanocarbon Materials

Ryu Obara[1], Hiroya Sasaki[1], Yasunori Chonan[1], Takao Komiyama[1], Koji Kotani[1]*, Hiroyuki Yamaguchi[1]*, Shigeru Yamauchi[2]*, Yasushi Sugawara[3], Takashi Sekine[3], Shigeaki Sugiyama[3], Yuichi Momoi[4]

[1]Faculty of Systems Science and Technology, Akita Prefectural University, Yurihonjo, Akita 015-0055, Japan

[2]Institute of Wood Technology, Akita Prefectural University, Noshiro, Akita 016-0876, Japan

[3]Akita Industrial Technology Center, Araya-cho, Akita 010-1623, Japan

[4]Toyo Corporation, Takatsuki, Osaka 569-0805, Japan

Corresponding author: Koji Kotani, kotani@akita-pu.ac.jp; Hiroyuki Yamaguchi, yamaguchi@akita-pu.ac.jp; Shigeru Yamauchi, sigeru@iwt.akita-pu.ac.jp

Abstract

We prepared binder-free monoliths of carbon nanohorns (CNHs), hole-opened carbon nanohorns (CNHoxs), multi-walled carbon nanotube (MWCNT), and single-walled carbon nanotube (SWCNT) using spark plasma sintering (SPS) method at 1800°C and 80 MPa in vacuum. The density of the SPS-treated SWCNT is 1.8 g/cm^3, which is close to that of graphite, while those of CNHs, CNHoxs, and MWCNT remained 1.1–1.3 g/cm^3 even after SPS treatment. We evaluated the monoliths using Raman spectroscopy and scanning electron microscopy observation, which showed a significant defect formation and graphitization of SWCNTs. Moreover, the increase of defect density in CNHs, CNHoxs, and MWCNT was moderate, and sub-micron size structures remained. We observed that the monoliths of CNHs and CNHoxs were highly conductive with a Hall mobility of positive holes of ~50 cm^2/Vs and electrical conductivity of ~300 S/cm. These experimental results indicated that the SPS treatment under appropriate conditions could provide CNHs monolith with nanostructure and good electrical conductivity.

Keywords

Carbon nanohorns
Spark plasma sintering
Raman spectroscopy
Nanostructure
Mobility
Electrical conductivity

1. Introduction

Nanocarbon materials such as carbon nanotubes (CNTs) and graphene have attracted much attention due to their unique physical and chemical properties, and have recently been actively studied for device applications such as sensors [1-9]. Carbon nonahorn (CNH) is a derivative of CNT. While single-walled CNTs (SWCNTs) have a cylindrical graphene-wrapped structure, CNHs have a horn-like structure with a graphene-wrapped and rounded tip.

Each CNH has a diameter of 2–5 nm and a length of about 40–50 nm and is produced as spherical aggregates (CNHs) of several thousand CNHs. The aggregates are almost uniform in size, with a diameter of approximately 100 nm [10]. Compared to CNTs, which are generally poorly dispersible, CNHs are dispersible in almost all organic solvents.

Oxidation of CNHs by heat and light energy results in porous CNH aggregates (CNHoxs) with holes in the wall [14]. CNHs and CNHoxs are reported to be free of metallic impurities and low in toxicity [15] since they do not use metal catalysts in their preparation as CNTs do, and they have also been studied for medical applications such as laser thermotherapy [15-17], and their application in the medical field, such as laser thermotherapy, is also being investigated [16,17]. It is also one of the nanocarbon materials that should be paid attention to in the future because it can be mass-produced and its material cost can be reduced.

Although a single independent CNT is known to have an extremely high carrier mobility of 104 cm^2/Vs or higher [18], the field-effect mobility of several thousand in the case of aligned CNTs and several tens of cm^2/Vs in the case of non-aligned CNTs have been reported [6,19,20]. It has been reported that Au nanoparticles at the nodes of CNT networks are effective in reducing sheet resistance [21,22].

While CNHs have been widely studied for energy devices, there are few reports on the electrical conductivity of CNHs themselves. The electrical conductivity of CNHs in powder form is 1.0–1.5 S/cm [23], and gas detection by electrical resistance change of CNH thin film has been reported as a sensor application [24,25]. In addition, the induced current by pulsed infrared light in composite films with poly(sodium 4-styrenesulfonate) (PSS) has been reported, and the mobility estimated from the transit time was as low as 3×10^{-9} cm^2/Vs [26,27]. This is interpreted to be due to the weak bonding between CNH molecules in the composite film. To speed up the sensor response speed and increase the electrical signal, it is necessary to suppress contact resistance and improve conductivity without damaging the nanostructure as much as possible.

We are aiming to improve the electrical conductivity of CNHs without adding impurities that could be scattering or trapping centers, so as not to impair the feature of CNHs that they do not contain metallic impurities. In this study, monoliths of CNHs, CNHoxs, multilayer CNTs (MWCNTs), and SWCNTs were fabricated by the spark plasma sintering (SPS) method and density evaluation, Raman spectroscopy, microstructure observation by scanning electron microscopy (SEM), and electrical properties were evaluated.

2. Sample preparation and experimental methods

In the SPS method, direct heating by Joule heat generated by applying a pulsed direct current (DC) while applying pressure to the raw powder packed in a graphite die is used. This enables sintering in a short time [28,29]. In this study, the SPS method was employed to strengthen intermolecular bonds and to suppress transformation and degradation caused by prolonged heating.

CNHs (185-2-1, NEC), CNHoxs (185-4, NEC), MWCNT (755133, Sigma-Aldrich), and SWCNT (698695, Sigma-Aldrich) powders were purchased and used as raw materials. The purity of CNHs and CNHoxs was 85%–95% (5%–15% graphite impurities), MWCNTs was 95% (5% metal oxides), and SWCNTs

had a carbon content of at least 70% with an unknown impurity composition. The SWCNT powder used here was not processed to separate semiconductors from metals.

Both samples were subjected to SPS treatment under the following conditions: pressure 80 MPa, temperature increase rate 50°C/min, sintering temperature 1,800°C, holding time 10 min, and in vacuum. The resulting monoliths were cut with a diamond cutter and surface polished with water-resistant abrasive paper (#1000, #1500), followed by lapping tape (#6000, #8000). The density was calculated from the volume and mass which were calculated from the dimensions. The molecular structure of the samples was evaluated from Raman spectroscopy. A Raman spectrometer (inVia Raman Microscope, Renishaw) was used to excite the sample with a laser beam of 532 nm wavelength and 15 mW energy intensity, and Raman spectra were measured in air with a resolution of 3 cm^{-1}. Microstructures were observed using a scanning electron microscope SEM (S-4300, Hitachi High-Tech) and compared before and after SPS treatment. The acceleration voltage was 15 kV. Electrical conductivity was evaluated using the Van der Pauw method. An electrode was attached to the sample with silver paste, and electrical resistance was measured at room temperature in air. Carrier concentration and mobility were evaluated from Hall effect measurements in air and at room temperature. A constant current of about 700 mA was applied to the sample and a magnetic field of up to 1 T was applied. The Hall coefficient was obtained from the magnetic field dependence of the Hall voltage. The carrier concentration and mobility were calculated using this and the measured electrical conductivity.

3. Experimental results and discussion

3.1. Density

Table 1 shows the densities before and after SPS treatment by specimen The densities of CNHs, CNHoxs, MWCNTs, and SWCNT monoliths after SPS treatment were 1.34, 1.13, 1.35, and 1.87 g/cm^3, respectively. The true densities of MWCNTs and SWCNTs were 2. The density of the SPS-treated SWCNTs was higher than the original true density, suggesting that they were transformed from SWCNTs into a different material. Considering that the densities of MWCNTs and graphite are 1.0–1.3 g/cm^3 and 1.8–2.0 g/cm^3 respectively in normal samples [30,31], SWCNTs were likely altered and graphitized by the SPS treatment. On the other hand, SPS-treated CNHs, CNHoxs, and MWCNTs were almost as dense as MWCNTs without SPS treatment. This suggests that the nanostructure-derived space created by winding graphene remains after SPS treatment.

3.2. Raman spectroscopy

Figure 1 (a-d) shows the Raman spectra of CNHs, CNHoxs, MWCNTs, and SWCNTs, respectively. The dashed lines correspond to before SPS treatment (raw powder) and the solid lines to after SPS treatment (monolith). In both cases, three characteristic peaks can be observed: D band (1350 cm^{-1}), G band (1580 cm^{-1}), and 2D band (2700 cm^{-1}). In general, the 2D band has a strong peak when the crystallinity is high and the number of layers is small, and broadens with an increase in the

Table 1. Density of nanocarbon before and after SPS treatment

Sample	Raw powder (g/cm^3)	SPS sample (g/cm^3)
CNHs	0.1 – 0.2	1.34
CNHoxs	0.2 – 0.3	1.13
MWCNT	0.005 – 0.014	1.35
SWCNT	0.02 – 0.15	1.87

number of layers, shifting toward higher energy [32,33].

Figure 1(a) shows that the G band peak intensity slightly decreased and the 2D band peak shifted from 2659 cm^{-1} to 2696 cm^{-1} in CNHs after SPS treatment. The G/D ratio also slightly decreased from 0.57 to 0.55 for CNHoxs, and the 2D band shifted from 2663 cm^{-1} to 2688 cm^{-1} (**Figure 1(b)**). **Figure 1(c)** shows that in the case of MWCNTs, the G/D ratio changed slightly from 0.88 to 0.85 and the 2D band shifted from 2672 cm^{-1} to 2690 cm^{-1}. The amount of the peak shift by SPS treatment is considered to be small. Compared to CNHs, CNHoxs, and MWCNTs, the Raman spectra of SWCNTs changed more significantly before and after SPS treatment (**Figure 1(d)**): the G/D ratio dramatically decreased from 7.9 to 2.4 and the 2D band shifted significantly from 2665 cm^{-1} to 2720 cm^{-1}. Furthermore, the Radical Breathing Mode (RBM) band, which is characteristic of SWCNTs and was observed around 100–300 cm^{-1} in the raw powder, disappeared after SPS treatment, suggesting that the SWCNT structure was severely lost.

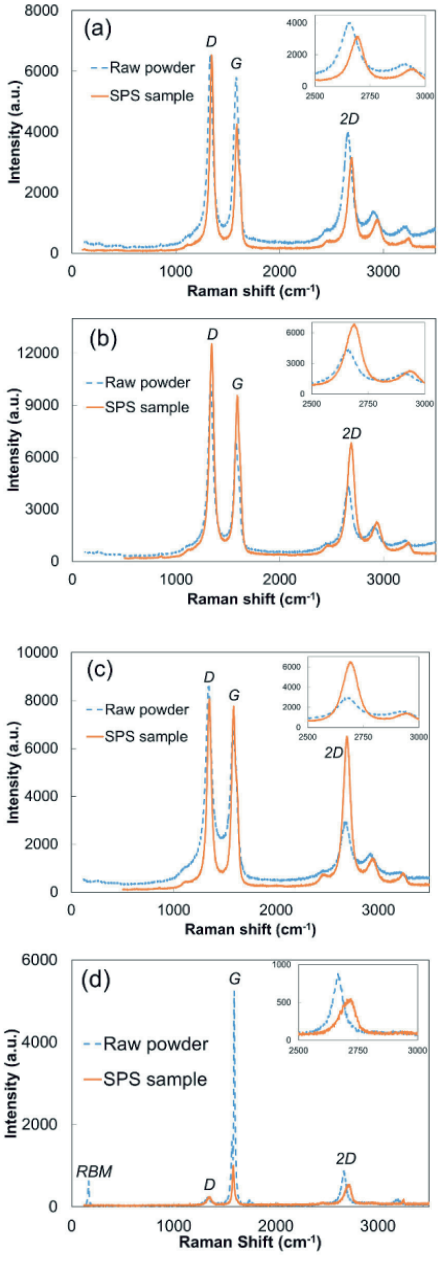

Figure 1. Raman spectra for the raw powders and SPS sample of **(a)** CNHs, **(b)** CNHoxs, **(c)** MWCNT, and **(d)** SWCNT. The inset showed an enlarged view of the 2D band.

The G/D ratios of CNHs, CNHoxs, MWCNTs, and SWCNTs before and after SPS treatment are summarized in **Table 2**. Although there are few detailed reports on the heat resistance of CNHs and CNHoxs, the above results are consistent with those reported in previous studies. As for the reason for the thermal stability of MWCNTs compared to SWCNTs, it may simply be that the outermost layer is multilayered, so that damage to the outermost layer has little effect on the inner layer, or that the multilayered outer layer has a larger radius, which reduces the local concentration of thermal energy. The multilayered nature of the nanotubes also reduces the localized concentration of thermal energy [34]. On the other hand, it has been reported that the heat resistance of nanotubes is reduced by defects and impurities [35]. Considering the above, the fact that CNHs are composed of thousands of CNHs in aggregates of about 100 nm and that CNHs do not contain metallic impurities may be related to the thermostability of CNHs. Further studies are needed to clarify these facts.

Table 2. G/D ratio in Raman spectra for nanocarbon before and after SPS treatment

Sample	G/D ratio	
	Raw powder	SPS sample
CNHs	0.79	0.70
CNHoxs	0.57	0.55
MWCNT	0.88	0.85
SWCNT	7.9	2.4

In general, the G/2D ratio of graphene provides information on the number of graphene layers or the stacking structure. According to Ferrari *et al.*, a strong peak appears around 2670 cm^{-1} when the number of graphene layers is small, but the peak shifts to around 2720 cm^{-1} when the number of layers increases to 5 or more and reaches graphite [36]. The Raman spectrum of CNTs becomes closer to the structure of graphite as the number of layers increases from monolayer to bilayer to multilayer, and the peak around 2700 cm^{-1} becomes stronger [37]. The results in **Figure 1** show that the G/H values of CNHs, CNHoxs, MWCNTs, and SWCNTs are similar to those of graphite, and were approximately 1 (0.92→0.98), 0.7 (1.1→0.79), 0.3 (2.3→0.73), and 0.3 (2.2→0.69) times higher, respectively, after SPS treatment than before treatment. The 2D peaks of CNHs, CNHoxs, MWCNTs, and SWCNTs were located around 2660–2670 cm^{-1} before SPS treatment; after SPS treatment, the peak positions for CNHs, CNHoxs and MWCNTs were 2690–2695 cm^{-1} for CNHs, CNHoxs, and MWCNTs, whereas only SWCNTs showed a large shift to the graphite peak at 2720 cm^{-1}. These results suggest that SPS treatment may have increased the number of layers. The reason for the difference in G/2D ratio between CNHs and CNHoxs, which increased about 1-fold, and MWCNTs, which increased about 0.3-fold, is unclear, but it is possible that the difference in molecular structure between urchin-like CNHs and fiber-like CNTs had an effect.

3.3. Microstructure

Figure 2 (a-d) shows SEM images of CNHs, CNHoxs, MWCNTs, and SWCNTs before and after SPS treatment. **Figure 2(a)1** and **(b)1** show that there are many spherical structures with a diameter of about 100 nm in the SEM images of the raw powder. In **Figure 2(c)1**, a fiber-like structure composed of many thin linear materials can be seen. In **Figure 2(d)1**, finer linear structures of different sizes can be seen intertwining with each other. Looking at the SEM images of the monoliths after SPS treatment in **Figure 2(a)2** and **(b)2**, it can be seen that rather large structures and small spherical structures coexist in both cases. In **Figure 2(c)2**, a rather large structure and a small fibrous structure coexist. In the Raman spectra of CNHs, CNHoxs, and MWCNTs, a slight decrease in the G/D ratio and a blue shift in the 2D band were observed after SPS treatment. These results can be interpreted as an increase in the number of layers and partial graphitization at the bonding interface due to the bonding of nanocarbon molecules with each other while maintaining the nanostructure. In contrast,

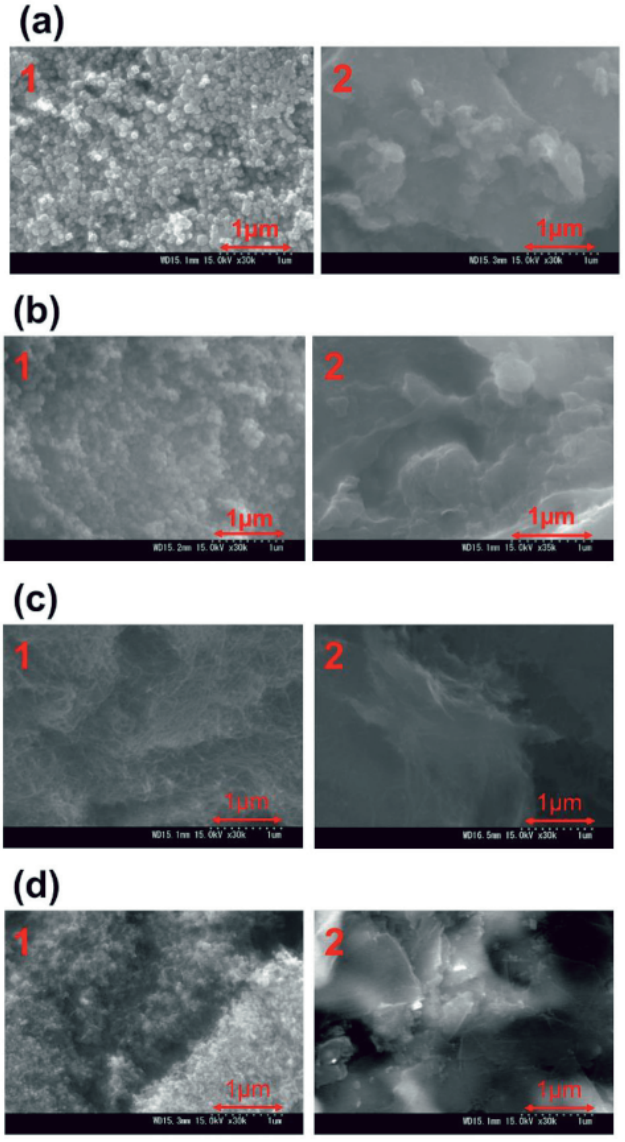

Figure 2. SEM images of the 1. raw powders and 2. SPS sample for **(a)** CNHs, **(b)** CNHoxs, **(c)** MWCNT, and **(d)** SWCNT

Table 3. Electrical conductivity, carrier density, mobility, and carrier type for the nanocarbon samples after SPS treatment

Raw powder	Electrical conductivity (S/cm)	Carrier density (cm^{-3})	Mobility (cm^2/Vs)	Type
CNHs	303	4.1×10^{19}	46	p
CNHoxs	280	3.4×10^{19}	53	p
MWCNT	329	1.2×10^{20}	18	p
SWCNT	2,098	3.8×10^{21}	4	p

Figure 2(d)2 shows that the SPS-treated monoliths of SWCNTs have a layered structure of microsize planar blocks, although some fibrous structure remains. The graphitization of the SWCNTs was severely enhanced by the SPS treatment. Yamamoto *et al.* reported that SPS treatment of SWCNTs at a sintering temperature of 1400°C and uniaxial pressure of 120 MPa causes tears and structural changes [38]. Considering the changes in density, Raman spectra, and microstructure obtained in this study, it is considered that the microstructure of SWCNTs is destroyed by SPS treatment and graphitization is advanced.

3.4. Electrical conductivity

Figure 3 shows the magnetic field dependence of the Hall voltage of SPS-treated CNHs, CNHoxs, MWCNTs, and SWCNTs. The conduction types were all p-type. The calculated conductivities and carrier mobility from these results are shown in **Table 3**. The conductivities of CNHs and CNHoxs monoliths after SPS treatment were 303 S/cm and 280 S/cm, respectively. Nitrogen doping is effective in improving the conductivity, and it has been reported that the conductivity can be increased up to 9 S/cm [39]. In this study, we found that SPS treatment can also improve bulk conductivity. This is thought to be due to the decrease in intermolecular contact resistance resulting from the strengthening of intermolecular bonds by SPS treatment. The carrier mobility of CNHs and CNHoxs was 46 cm^2/Vs and 53 cm^2/Vs, respectively. The carrier concentration of CNHoxs was lower than that of CNHs, suggesting the possibility of carrier trapping in the open pores. On the other hand, the electrical conductivity of the MWCNT monoliths was 329 S/cm and the carrier mobility was only 18 cm^2/Vs. The SWCNTs are considered to be considerably graphitized after SPS treatment. The electrical conductivity of 2098 S/cm is a reasonable value for graphite. The mobility of 4 cm^2/Vs is the lowest among the four samples, but the monolith obtained in this study is unoriented unlike highly oriented pyrolytic graphite (HOPG) [31], and the defect concentration increased significantly during SPS treatment, as shown by the marked decrease in the G/D ratio in the Raman spectra, and these two factors may be responsible for the low mobility. The two factors are thought to be the cause of the low mobility.

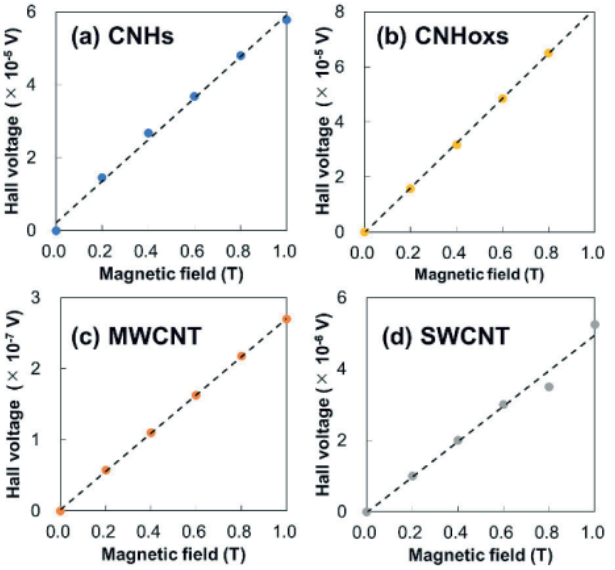

Figure 3. Magnetic field dependence of Hall voltage in **(a)** CNHs, **(b)** CNHoxs, **(c)** MWCNT, and **(d)** SWCNT samples after SPS treatment

4. Conclusion

CNHs, CNHoxs, MWCNTs, and SWCNT powders were subjected to SPS treatment, and free-standing monoliths were fabricated without adding impurities that

could serve as scattering or trapping centers. Density evaluation, Raman spectroscopy, SEM observation, and conductivity evaluation were performed on these monoliths. The density of SWCNTs treated by SPS under the following conditions: pressure 80 MPa, temperature increase rate 50°C/min, sintering temperature 1800°C, holding time 10 min, and vacuum was 1.87 g/cm^3, which is close to that of graphite (1.8–2.0 g/cm^3). On the other hand, CNHs, CNHoxs, and MWCNTs showed values of 1.13–1.35 g/cm^3 after SPS treatment. Raman spectroscopy and SEM observations showed that SWCNTs were generally graphitized and lost their nanostructures due to SPS treatment, resulting in many defects. On the other hand, CNHs, CNHoxs, and MWCNTs showed good electrical conductivity of 300 S/cm and carrier mobility of 50 cm^2/Vs, while retaining their nanostructures.

Disclosure statement

The authors declare no conflict of interest.

References

[1] Seike K, Fujii Y, Ohno Y, et al., 2014, Floating-Gated Memory Based on Carbon Nanotube Field-Effect Transistors with Si Floating Dots. Jpn J Appl Phys 53: 04EN07.

[2] Nosho Y, Ohno Y, Kishimoto S, et al., 2007, Evidence of Edge Conduction at Nanotube/Metal Contact in Carbon Nanotube Devices. Jpn J Appl Phys, 46: L474.

[3] Cai X, Sushkov AB, Suess RJ, et al., 2014, Sensitive Room-Temperature Terahertz Detection via the Photothermoelectric Effect in Graphene. Nat Nanotechnol, 9: 814–819.

[4] St-Antoine BC, Ménard D, Martel R, 2011, Single-Walled Carbon Nanotube Thermopile For Broadband Light Detection. Nano Lett, 11(2): 609–613.

[5] Suzuki D, Oda S, Kawano Y, 2016, A Flexible and Wearable Terahertz Scanner. Nat Photonics, 10(12): 809–813.

[6] Sarker BK, Kang N, Khondaker SI, 2014, High Performance Semiconducting Enriched Carbon Nanotube Thin Film Transistors Using Metallic Carbon Nanotubes as Electrodes. Nanoscale, 6: 4896–4902.

[7] Zaumseil J, 2015, Single-Walled Carbon Nanotube Networks for Flexible and Printed Electronics. Semicond Sci Technol, 30: 074001.

[8] Yoon J, Lee D, Kim C, et al., 2014, Accurate Extraction of Mobility in Carbon Nanotube Network Transistors Using C-V and I-V Measurements. Appl Phys Lett, 105: 212103.

[9] Xu H, Chen L, Hu L, et al., 2010, Contact Resistance of Flexible, Transparent Carbon Nanotube Films with Metals. Appl Phys Lett, 97: 143116.

[10] Iijima S, Yudasaka M, Yamada R, et al., 1999, Nano-Aggregates of Single-Walled Graphitic Carbon Nano-Horns. Chem Phys Lett, 309(3–4): 165–170.

[11] Yuge R, Miyawaki J, Ichihashi T, et al., 2010, Highly Efficient Field Emission from Carbon Nanotube-Nanohorn Hybrids Prepared by Chemical Vapor Deposition. ACS Nano, 4(12): 7337–7343.

[12] Yuge R, Ichihashi T, Shimakawa Y, et al., 2004, Preferential Deposition of Pt Nanoparticles Inside Single-Walled Carbon Nanohorns. Adv Mater, 16(16): 1420–1423.

[13] Yuge R, Nihey F, Toyama K, et al., 2017, Carbon Nanotubes Forming Cores of Fibrous Aggregates of Carbon Nanohorns. Carbon, 122: 665–668.

[14] Utsumi S, Miyawaki J, Tanaka H, et al., 2005, Opening Mechanism of Internal Nanoporosity of Single-Wall Carbon Nanohorn. J Phys Chem B, 109(30): 14319–14324.

[15] Miyawaki J, Yudasaka M, Azami T, et al., 2008, Toxicity of Single-Walled Carbon Nanohorns. ACS Nano, 2(2): 213–226.

[16] Miyako E, Deguchi T, Nakajima Y, et al., 2012, Photothermic Regulation of Gene Expression Triggered by Laser-Induced Carbon Nanohorns. Proc Natl Acad Sci USA, 109(19): 7523–7528.

[17] Whitney JR, Sarkar S, Zhang J, et al., 2011, Single Walled Carbon Nanohorns as Photothermal Cancer Agents. Lasers Surg Med, 43(1): 43–51.

[18] Dürkop T, Getty SA, Cobas E, et al., 2004, Extraordinary Mobility in Semiconducting Carbon Nanotubes. Nano Letters, 4(1): 35–39.

[19] Snow ES, Campbell PM, Ancona MG, et al., 2005, High-Mobility Carbon-Nanotube Thin-Film Transistors on a Polymeric Substrate. Appl Phys Lett, 86: 033105.

[20] Cai L, Wang C, 2015, Carbon Nanotube Flexible and Stretchable Electronics. Nanoscale Research Letters, 10: 320.

[21] Velamakanni A, Magnuson CW, Ganesh KJ, et al., 2010, Site-Specific Deposition of Au Nanoparticles in CNT Films by Chemical Bonding. ACS Nano, 4(1): 540–546.

[22] Tian X, Moser ML, Pekker A, et al., 2014, Effect of Atomic Interconnects on Percolation in Single-Walled Carbon Nanotube Thin Film Networks. Nano Lett, 14(7): 3930–3937.

[23] NEC Corporation. Carbon Nanohorns, 2017. Viewed 16 June 2020. https://www.nec.com/en/global/prod/cnh/pdf/CarbonNanohorn.pdf

[24] Suehiro J, Sano N, Zhou G, et al., 2006, Application of Dielectrophoresis to Fabrication of Carbon Nanohorn Gas Sensor. Journal of Electrostatics, 64(6): 408–415.

[25] Urita K, Seki S, Utsumi S, et al., 2006, Effects of Gas Adsorption on the Electrical Conductivity of Single-Wall Carbon Nanohorns. Nano Lett, 6(7): 1325–1328.

[26] Obara R, Chonan Y, Komiyama T, et al., 2020, Infrared Photoresponse of Oxidized Carbon Nanohorns: PSS Composite Films. Jpn J Appl Phys, 59: SGGK01.

[27] Tameev AR, Jiménez LL, Pereshivko LY, et al., 2007, Charge Carrier Mobility in Films of Carbon-Nanotube-Polymer Composites. J Phys: Conf Ser, 61: 1152–1156.

[28] Sekine T, Nino A, Sugawara Y, et al., 2019, Effects of Transition Metal Carbides (NbC, TaC, WC, ZrC) on Mechanical Properties of TiC-SiC Composite Ceramics. J Jpn Soc Powder Powder Metallurgy, 66: 530–535.

[29] Sugawara Y, Sugiyama S, Fuda K, 2019, Formation of Magneli Phase and Its Influence on Thermoelectric Properties in Preparation of TiO_2-TiB_2 Thermoelectric Compacts Fabricated by Spark Plasma Sintering. J Jpn Soc Powder Powder Metallurgy, 66: 323–329.

[30] New Energy and Industrial Technology Development Organization. All About Carbon Nanotubes, 2016, Nikkan Kogyo Shimbun, Tokyo.

[31] Murakami M, 2014, Graphene and Thin Films from the Viewpoint of Graphite. Production and Technology, 66: 3.

[32] Avouris P, Heinz TF, Low T. 2D Materials: Properties and Devices, 2017, Cambridge University Press, Cambridge.

[33] Dresselhaus MS, Jorio A, Hofmann M, et al., 2010, Perspectives on Carbon Nanotubes and Graphene Raman Spectroscopy. Nano Lett, 10: 751–758.

[34] Xu F, Sun LX, Zhang J, et al., 2010, Thermal Stability of Carbon Nanotubes. J Therm Anal Calorim, 102: 785–791.

[35] Davoodi J, Soleymani M, Alizade Sabet H, 2018, Thermal Stability of Single Walled SiGe Nanotube with Vacancy Defects: a Molecular Dynamics Simulation Study. Silicon, 10: 731–736.

[36] Ferrari AC, Meyer JC, Scardaci V, et al., 2006, Raman Spectrum of Graphene and Graphene Layers. Phys Rev Lett,

97: 187401.

[37] Fujisawa K, 2014, Comparison of Raman Spectra of Various Carbon Materials. Nagano Prefectural Industrial Technology Center Research Report, 9: 33–35.

[38] Yamamoto T, Sato Y, Takahashi T, et al., 2005, Mechanical Properties of Solidified Single-Walled Carbon Nanotube Bulks Prepared by Discharge Plasma Sintering. Transactions of the Japan Society of Mechanical Engineers, 71: 330.

[39] Kurungot S, Unni SM, Ramadas S, 2014, A Process for the Preparation of Nitrogen Doped Carbon Nanohorns for Oxygen Reduction Electrocatalysis. European Patent Specification, 2014: EP3060519B1.